

Mapping gaseous dimethylamine, trimethylamine, ammonia, and their particulate counterparts in marine atmospheres of China's marginal seas: Part 1 - Differentiating marine emission from continental transport

5 Dihui Chen¹, Yanjie Shen¹, Juntao Wang¹, Yang Gao^{1,2}, Huiwang Gao^{1,2}, Xiaohong Yao^{1,2*}

¹Key Laboratory of Marine Environment and Ecology, and Frontiers Science Center for Deep Ocean Multispheres and Earth System, Ministry of Education, Ocean University of China, Qingdao 266100, China

²Laboratory for Marine Ecology and Environmental Science, Qingdao National Laboratory for Marine Science and Technology, Qingdao 266237, China

10 * *correspondence to:* Xiaohong Yao (xhyao@ouc.edu.cn)

Abstract. To study sea-derived gaseous amines, ammonia, and primary particulate aminium ions in the marine atmosphere of China's marginal seas, an onboard URG-9000D Ambient Ion Monitor-Ion chromatography (AIM-IC, Thermo Fisher) was set up on the front deck of the R/V Dongfanghong 3 to semi-continuously measure the spatiotemporal variations in the concentrations of atmospheric trimethylamine (TMA_{gas}), dimethylamine (DMA_{gas}), and ammonia (NH_{3gas}) along with their particulate matter (PM_{2.5}) counterparts. In this study, we differentiated marine emissions of the gas species from continental transport using data obtained from December 9 to 22, 2019 during the cruise over the Yellow and Bohai seas, facilitated by additional short-term measurements collected at a coastal site near the Yellow Sea during summer, fall, and winter of 2019. The data obtained from the cruise and coastal sites demonstrated that the observed TMA_{gas} and protonated trimethylamine (TMAH⁺) in PM_{2.5} over the Yellow and Bohai seas overwhelmingly originated from marine sources. During the cruise, there was no significant correlation (P>0.05) was observed between the simultaneously measured TMAH⁺ and TMA_{gas} concentrations. Additionally, the concentrations of TMAH⁺ in the marine atmosphere varied around 0.28±0.18 µg m⁻³ (average ± standard deviation), with several episodic hourly average values exceeding 1 µg m⁻³, which were approximately one order of magnitude larger than those of TMA_{gas} (approximately 0.031±0.009 µg m⁻³). Moreover, there was a significant negative correlation (P<0.01) between the concentrations of TMAH⁺ and NH₄⁺ in PM_{2.5} during the cruise. Therefore, the observed TMAH⁺ in PM_{2.5} was overwhelmingly derived from primary sea-spray aerosols. Using the TMA_{gas} and TMAH⁺ in

15

20

25

PM_{2.5} as tracers for sea-derived basic gases and sea-spray particulate aminium ions, the values of non-sea-derived DMA_{gas}⁺, and NH_{3gas}, and non-sea-spray particulate DMAH⁺ in PM_{2.5}, were estimated. The estimated average values of each species contributed to 16%, 34%, and 65% of the observed average concentrations for non-sea-derived DMA_{gas}, NH_{3gas} and non-sea-spray particulate DMAH⁺ in PM_{2.5}, respectively. Uncertainties remained in the estimations, as TMAH⁺ may decompose into smaller molecules in seawater to varying extents. The non-sea-derived gases and non-sea-spray particulate DMAH⁺ likely originated from long-range transport from the upwind continents, based on the recorded offshore winds and increased concentrations of non-sea-salt SO₄²⁻ (nss-SO₄²⁻) and NH₄⁺ in PM_{2.5}. The lack of a detectable increase in the particulate DMAH⁺, NH₄⁺, and nss-SO₄²⁻ concentrations in several SO₂ plumes did not support the secondary formation of particulate DMAH⁺ in the marine atmosphere.

35 **Keywords:** Marine atmospheric NH₃, trimethylamine, dimethylamine, particulate aminium, sea-spray aerosol

1. Introduction

Gaseous amines and their particulate counterparts are vital for reduced nitrogen compounds in the marine atmosphere (Facchini et al., 2008; Müller et al., 2009; Hu et al., 2015; Hu et al., 2018; van Pinxteren et al., 2015; van Pinxteren et al., 2019; Yu et al., 2016; Xie et al., 2018; Zhou et al., 2019) and are primarily derived from the seawater, where glycine betaine (GBT), trimethylamine N-oxide (TMAO), and choline are the three major precursors (Burg and Ferraris, 2008; Lidbury et al., 2015a; Lidbury et al., 2015b; Jameson et al., 2016; Taubert et al., 2017). GBT, TMAO, and choline are critical for maintaining the osmotic pressure in marine organisms. When released into the environment, they can be degraded by bacteria to trimethylamine (TMA), and then dimethylamine (DMA), or methylamines (MA) (Lidbury et al., 2015a; Lidbury et al., 2015b). Gaseous DMA, TMA, and MA may be vital in the formation of secondary particles in the atmosphere by nucleation (Almeida et al., 2013; Chen et al., 2016; Yao et al., 2018; Zhu et al., 2019). In addition to biogenic emissions of amines, anthropogenic emissions are known as important sources of amines in the continental atmosphere, but not in the marine atmosphere (Ge et al., 2011). Modeling studies have shown that the continental amine species in gas and/or particle phases can be transported regionally, including downwind marine atmospheres (Yu and Luo, 2014; Mao et al., 2018).

Simultaneous real-time measurement of gaseous amines and their particulate counterparts in the marine atmosphere over the ocean remains challenging because of artifact signals related to self-vessel emissions and amine-contained dew evaporation; however, this is not the case in the continental atmosphere (VandenBoer et al., 2011). The lack of direct measurements restricts the determination of their sources and the relationship between the reduced nitrogen compounds and acid-base neutralization reactions in the marine atmosphere.

Reduced nitrogen compounds in the ocean can finally decompose into ammonium ions (NH_4^+) and other smaller molecules. NH_4^+ in surface seawater releases to the marine atmosphere as atmospheric ammonia ($\text{NH}_{3\text{gas}}$) under favorable conditions (Johnson et al., 2008; Carpenter et al., 2012; Paulot et al., 2015). The ocean is an important source of $\text{NH}_{3\text{gas}}$, contributing to approximately 40% of the natural NH_3 emissions on Earth (Carpenter et al., 2012; Paulot et al., 2015). In the literature, large uncertainties remain in estimating NH_3 emissions from the ocean; for example, the annual emission flux ranges from 2 to 23 Tg N a^{-1} (Clarke and Porter, 1993; Dentener and Crutzen, 1994; Sutton et al., 2013; Paulot et al., 2015). These uncertainties are primarily derived from two factors: 1) the major marine sources of $\text{NH}_{3\text{gas}}$ are still disputed, such as seawater, sea birds, or the photolysis of marine organic nitrogen at the ocean's surface or in the atmosphere; and 2) direct $\text{NH}_{3\text{gas}}$ observations in marine atmospheres are restricted as onboard ambient $\text{NH}_{3\text{gas}}$ measurement techniques sometimes suffer from large artifacts from $\text{NH}_{3\text{gas}}$ contamination associated with onboard human activities, dew evaporation, and water vapor interference (Quinn et al., 1990; Clarke and Porter, 1993; Johnson et al., 2008; Keene et al., 2009; Wentworth et al., 2016; Teng et al., 2017). Additionally, the long-range transport of atmospheric $\text{NH}_{3\text{gas}}$ from the continent may also complicate the source analysis of $\text{NH}_{3\text{gas}}$ in marine atmospheres (McNaughton et al., 2004; Uematsu et al., 2004; Zhao et al., 2015; Lutsch et al., 2016).

To identify and characterize sea-derived gaseous amines, ammonia, and sea-spray particulate ammonium ions, as well as secondary particulate ammonium ions from continental transport in the atmospheres of China's marginal seas, we conducted two cruise campaigns: one over the Yellow and Bohai seas in China from December 9 to 22, 2019 (Campaign A), and another over the Eastern China and Yellow seas from December 27, 2019, to January 16, 2020 (Campaign B). Winter cruise campaigns provide great opportunities for observational studies due to the following: 1) higher concentrations of nutrients in the seas at a lower sea surface water temperatures, which may favor higher primary production (Guo et al., 2020) and subsequently increase marine emissions of gaseous amines and/or ammonium-contained sea-spray aerosols; 2) periodically

enhanced air-sea exchanges driven by the strong winter Asian monsoon every 4–10 days (Zhu et al., 2018); and 3) periodically enhanced long-range transport of anthropogenic pollutants from continents to the seas, which may enhance the formation of secondary ammonium and aminium aerosols (Guo et al., 2016; Yu et al., 2016; Xie et al., 2018; Wang et al., 2019).

In this study, an onboard URG-9000D Ambient Ion Monitor-Ion chromatography (AIM-IC, Thermo Fisher) instrument was used to simultaneously measure the spatiotemporal variations in the concentrations of gaseous amines and $\text{NH}_{3\text{gas}}$, along with their counterparts in $\text{PM}_{2.5}$. Semi-continuous measurement data were then analyzed to identify the study targets. This study was divided into two parts. In this section, we distinguish the marine sources from the continental transport of reduced nitrogen compounds in marine atmospheres and subsequently quantify each contribution to the observed species during the December 9-22, 2019 campaign. In the companion paper (Gao et al., 2021), we analyzed the spatiotemporal heterogeneity and related causes, and subsequently delivered a hypothesis regarding the marine emissions of reduced nitrogen compounds using the data from the two campaigns and data from an additional cruise campaign previously reported by Hu et al. (2015).

2. Experimental

2.1 Sampling periods, locations, and instruments

Campaign A was conducted from December 9 to 19, 2019, on the R/V Dongfanghong-3 with a displacement tonnage of 5000. The research vessel was still within its testing period and used state-of-the-art combustion technology with low-sulfur diesel. Campaign B started from December 27, 2019, to January 17, 2020, and was organized by another research team. During December 20-22, the vessel was anchored at the port while the sampling continued. The 44 hours were referred to as the transition period between campaigns A and B. A standard-sized air-conditioned container was set up on the front deck to house a suite of instruments including the AIM-IC, a fast-mobility particle sizer (FMPS, Tsi), a cloud condensation nuclei counter (CCN-100, Droplet MT), and a single particle aerosol mass spectrometer (SPAMS 05, Hexin) etc., for measuring the air pollutant concentrations. No human activities occurred on the front deck during cruising, excluding anchoring at the port. Even during the anchoring period, human activity on the front deck was rare. The use of the container on the front deck effectively minimized the self-vessel contamination by $\text{NH}_{3\text{gas}}$ and gaseous amines. The front deck was approximately 10 m

above sea level, and the container height was 2.8 m.

To ensure that the onboard AIM-IC was operated properly, it was housed in a mobile air-conditioned mini-container, which was further placed in a standard container with a 1 m stainless steel sampling probe connected to the ambient air. The inlet of the sampling probe extended from the top corner of the standard container facing the sea. The AIM-IC consists of two major parts: an ambient air sampling system and an ion chromatography analysis system. For the sampling system, the AIM-IC was equipped with a PM_{2.5} cyclone and operated at a rate of 3 L/min. The sampled gases and particles in the water solution were stored in two syringes prior to their injection for analysis. The ion chromatography analysis system measured the semi-continuous concentrations of chemically reactive gases. These included NH_{3gas}, gaseous amines, and acidic gases such as SO₂ and HNO₃, along with their particulate counterparts, at a temporal resolution of 1 h. This facilitated the identification of possible interference from onboard dew evaporation, which typically occurs with sunrise (Teng et al., 2017).

An automatic weather system providing real-time meteorological data is available on the R/V Dongfanghong-3. The heading wind was corrected to determine the true wind speed and direction. The surface seawater temperature was not measured during this cruise campaign, and typically had a delay of a few hours when compared to the ambient air temperature (Deng et al., 2014).

On August 1-9, September 12 to October 1, and November 16 to December 1, 2019, the AIM-IC was set up at a coastal site in Qingdao (36.34° N, 120.67° E) to conduct routine measurements (Fig. 1). Coastal measurement data were obtained from two weeks to four months before the winter cruise campaign. The sampling site was located in a new high-technology zone near the Yellow Sea, with the shortest distance from the sea being approximately 1 km in the south. The AIM-IC was housed in a research lab on the fifth floor of a building, approximately 16 m above ground level. The sampling probe extended out of the window and was directly connected to the ambient air. Typically, higher biogenic emissions of reduced nitrogen compounds over the continents are expected in the summer than in the winter owing to the temperature effect (Yu et al., 2016; Teng et al., 2017).

2.2 Chemical analysis

The AIM-IC includes an ICS-1100 ion chromatograph, wherein an analytical column (Ion Pac CS17A (2×250 mm)) was

used to measure cations, including Na^+ , NH_4^+ , protonated dimethylamine (DMAH^+), and protonated trimethylamine (TMAH^+), and an AS11-HC (2×50 mm) was used to measure anions, including SO_4^{2-} , NO_3^- , Cl^- , and organic ions. Methanesulfonic acid solution (5 mM) was used as the eluent for cation analysis, while potassium hydroxide solution, (varying from 3 to 40 mM), was used as the gradient eluent for anion analysis. Each analysis took 26-28 mins to obtain a complete ion spectrum. The volume of the injection loop installed on the low-pressure valve was 250 μL , which substantially reduced the limits of detection for all ions. The limits of detection for NH_4^+ , DMAH^+ , and TMAH^+ were 0.0004, 0.004, and 0.002 $\mu\text{g m}^{-3}$, respectively, in ambient air, respectively. The limits of detection for NO_3^- and SO_4^{2-} were 0.05 and 0.015 $\mu\text{g m}^{-3}$, respectively, in ambient air. The ICS-1100 was calibrated onboard prior to obtaining regular measurements, and the second calibration was conducted when the vessel was anchored at the port. The AIM-IC analysis was not affected by ambient water vapor, as the device directly measured the ions. Detailed information regarding the AIM-IC analysis is provided in the studies of Teng et al. (2017) and Xie et al. (2018). Notably, strong K^+ interference occurred unexpectedly and occasionally, and then disappeared during different campaigns. When the interference occurred, DMAH^+ and TMAH^+ were undetectable because of the increased baseline at the corresponding residence time in the ion chromatograph (Fig. S1); consequently, some $\text{PM}_{2.5}$ DMAH^+ and TMAH^+ concentration data are unavailable in Fig. 1. However, the concentrations of gaseous amines were still detected correctly, with a low baseline at the residence. The K^+ interference remains to be investigated. Additionally, a few surface seawater samples were also collected from different sea zones. The NH_4^+ and ammonium ion concentrations in the samples were not measured, as the analytical methods were still hindered by high sea-salt ion contents.

140 3. Results

3.1 Temporal variations in the concentrations of basic gases and their $\text{PM}_{2.5}$ counterparts in the coastal atmosphere

Before analyzing the basic gases and their counterparts in the marine atmosphere, we initially presented their continental concentrations at the coastal site facing the Yellow Sea, as these observations provide important evidence to facilitate the analysis of the contributors to these species in the marine atmosphere. Figs. 1a & b show that the TMA_{gas} and TMAH^+ concentrations in $\text{PM}_{2.5}$ were mostly below the detection limit, varying at approximately $0.001 \pm 0.001 \mu\text{g m}^{-3}$ (average \pm standard deviation), regardless of the presence of offshore or onshore winds during short-term measurements in the three

seasons of 2019. The DMA_{gas} and DMAH⁺ concentrations varied at 0.018±0.021 and 0.017±0.013 μg m⁻³, respectively, which were approximately one order of magnitude larger than those of TMA_{gas} and TMAH⁺. TMA_{gas} and TMAH⁺ concentrations in the upwind continental and coastal atmospheres were substantially lower than those reported in the literature, by up to a few tens of ng m⁻³ (Ge et al., 2011). However, Gibb et al. (1999) reported a low average TMA_{gas} (0.5 ng m⁻³) and particulate TMAH⁺ (0.5 ng m⁻³) in the marine atmosphere over the Arabian Sea on November 16 to December 19, 1994. Xie et al. (2018) reported that TMAH⁺ concentrations were comparable to those of DMAH⁺ in atmospheric particles collected at two other coastal sites located approximately 20 km from the study area, as listed in Table S1. The cause of this change is beyond the scope of this study, but may be due to the large decrease in manure application, based on our recent survey in the Qingdao area.

The DMA_{gas} and DMAH⁺ concentrations in PM_{2.5} concentrations with offshore winds from the north were substantially higher than those with onshore winds from the south or southeast (the top of Fig. 1a), suggesting that their continental emissions and related secondary sources were stronger. Moreover, the concentrations of DMA_{gas} and DMAH⁺ were moderately correlated with those of NH_{3gas} and NH₄⁺; namely, [DMA_{gas}] = 5.6 × 10⁻³ × [NH_{3gas}] (R²=0.79, P<0.01), and [DMAH⁺]_{PM2.5}=5.9 × 10⁻³ × [NH₄⁺]_{PM2.5} (R²=0.84, P<0.01). Generally, the DMA_{gas} and DMAH⁺ concentrations were approximately 1/200 of those of the corresponding NH_{3gas} and NH₄⁺.

3.2 Spatiotemporal variations in the concentrations of basic gases over the seas

Throughout Campaign A, the TMA_{gas} concentrations varied at approximately 0.031±0.009 μg m⁻³ (Figs. 2a-c), with three peaks occurring at 4–5 day intervals (gray shadowing in Fig. 2c). Peaks 1 and 2 were generally associated with offshore winds, while peak 3 was mostly associated with onshore winds (Fig. 2b). The peaks lasted from tens to dozens of hours and were not induced by the onboard dew evaporation at sunrise. For example, the highest value (0.060 μg m⁻³) occurred at 23:00 on December 16. The observed TMA_{gas} concentrations were one order of magnitude higher than those measured in the coastal atmosphere during the summer, fall, and winter. This suggested that the TMA_{gas} observed during Campaign A was largely derived from marine sources rather than from long-range continental transport. The same conclusion can be drawn by analyzing the three peaks of TMA_{gas} and its temporal variations during the anchoring port period. For example, during peak

1 (Fig. 2a), the concentrations of TMA_{gas} increased by approximately 100% from 20:00 on December 9 to 11:00 on December 10, with an approximately 30% decrease in the non-sea-salt SO₄²⁻ (nss-SO₄²⁻) concentration (from 22 to 16 μg m⁻³; Fig. 2b). Moreover, the peaks in the TMA_{gas} concentrations corresponded to troughs in the nss-SO₄²⁻ concentrations during peak 3, as shown in Figs. 2c & d. The self-vessel emissions of nss-SO₄²⁻ in PM_{2.5} were negligible because of the use of low-sulfur diesel, which is discussed later. The increased nss-SO₄²⁻ concentrations in PM_{2.5} may be a good indicator of continental transport, and vice versa.

The concentrations of DMA_{gas} varied at approximately 0.006±0.006 μg m⁻³ (Fig. 2d) and were significantly higher than those of TMA_{gas} (P<0.01). Unlike TMA_{gas}, continental transport was likely acted as an important contributor to the DMA_{gas} and NH_{3gas} observed in the marine atmosphere, particularly during peak 1, when higher nss-SO₄²⁻ concentrations were observed in PM_{2.5} (Figs. 2c-e). The DMA_{gas} and NH_{3gas} concentrations were negatively correlated with those of TMA_{gas} during peak 1; namely, R²=0.35 (P<0.01) between TMA_{gas} and DMA_{gas}, and R²=0.17 (P<0.01) between TMA_{gas} and NH_{3gas}. This suggested that most of the DMA_{gas} and NH_{3gas} were likely derived from continental transport, rather than marine sources. During peak 2, increased TMA_{gas}, DMA_{gas}, and NH_{3gas} concentrations were concurrently observed with increasing nss-SO₄²⁻ concentrations, suggesting that both the marine emissions and continental transport simultaneously contributed to the observed DMA_{gas} and NH_{3gas} at the same time moment. During the port-anchoring period from December 20-22, the DMA_{gas} and NH_{3gas} concentrations varied slightly, and were moderate and low, respectively. However, the TMA_{gas} concentrations continuously increased by over 100% as the ambient temperature increased (Figs. 2c and f). Additionally, the nss-SO₄²⁻ concentrations of PM_{2.5} varied greatly and followed a bell-shaped pattern during the port-anchoring period.

Additionally, the NH_{3gas} concentrations varied at approximately 0.53 ± 0.53 μg m⁻³ from December 9-22. The variation narrowed to approximately 0.24 ± 0.07 μg m⁻³ during the port-anchoring period from December 20-22. When the data during Campaign A were used for the analysis, the NH_{3gas} concentrations were significantly correlated with those of DMA_{gas}; namely, [DMA_{gas}] = 9.2 × 10⁻³ × [NH_{3gas}] (R²=0.71, P<0.01). However, there was no correlation between the NH_{3gas} and TMA_{gas} concentrations.

3.3 Spatiotemporal variations in the aminium and NH_4^+ ion concentrations of $\text{PM}_{2.5}$ over the seas

195 Figs. 3a-f show the spatiotemporal variations in the TMAH^+ , DMAH^+ , and NH_4^+ concentrations of $\text{PM}_{2.5}$ throughout Campaign A from December 9–22, during which the TMAH^+ concentrations varied greatly at approximately $0.28 \pm 0.18 \mu\text{g m}^{-3}$. However, they narrowed at approximately $0.21 \pm 0.04 \mu\text{g m}^{-3}$ during the port-anchoring period. The TMAH^+ concentrations generally increased from $0.13 \pm 0.05 \mu\text{g m}^{-3}$ on December 9 to $0.46 \pm 0.05 \mu\text{g m}^{-3}$ on December 16 (Fig. 3a), and subsequently decreased to approximately $0.2 \mu\text{g m}^{-3}$ thereafter, excluding some strong peaks from 0.62 – $1.24 \mu\text{g m}^{-3}$ at 200 03:00–05:59 and 1.02 – $1.81 \mu\text{g m}^{-3}$ at 14:00–16:59 on December 18 (grey shadowing representing peak 4 in Figs. 3a-d). The peaks reproduced the episodes observed in the marine atmosphere over the Yellow Sea in May 2012 (Hu et al., 2015) and were repeatedly observed during Campaign B (Gao et al., 2021). However, they were not observed in the several other marine cruise campaigns conducted across the marginal seas of China and the northwestern Pacific Ocean (Hu et al., 2018; Xie et al., 2018).

205 As the TMAH^+ concentrations were approximately two orders of magnitude higher than those observed at the coastal site during the three seasons of 2019, the observed TMAH^+ was likely largely derived from marine sources. The TMAH^+ concentrations followed a spatiotemporal pattern that was clearly differed from those of DMAH^+ and NH_4^+ , while the latter two ions exhibited a similar spatiotemporal pattern during most of the periods of Campaign A (Figs. 3a-c). A significant negative correlation ($P < 0.01$) was observed between the concentrations of TMAH^+ and NH_4^+ in $\text{PM}_{2.5}$ (not shown). The spatiotemporal pattern of the TMAH^+ concentration also significantly differed from those of nss-SO_4^{2-} (Fig. 2d) and SO_2 (Fig. 3b), which are regarded as the tracers of long-range transported continental pollutants and fresh vessel plumes. For example, the extremely strong TMAH^+ peaks occurred concurrently with low nss-SO_4^{2-} , NH_4^+ , and SO_2 concentrations, accompanied by high Na^+ concentrations under high wind speeds, which are common indicators of sea spray aerosols (Feng et al., 2017). Moreover, the TMAH^+ concentrations were approximately one order of magnitude larger than those of TMA_{gas} , and no significant correlation was observed between them ($P > 0.05$). This suggests that the observed TMAH^+ may not be derived 215 from the neutralization reactions of TMA_{gas} with acids in the marine atmosphere, and may have been derived from primary sea-spray organic aerosols (Hu et al., 2015, 2018). Primary sea-spray organic aerosols mainly contain primary and degraded

biogenic organics (Ault et al., 2013; Prather et al., 2013; Quinn et al., 2015; Dall'Osto et al., 2019).

The DMAH⁺ concentrations varied at approximately $0.065 \pm 0.068 \mu\text{g m}^{-3}$ from December 9-22; however, they varied at approximately $0.10 \pm 0.04 \mu\text{g m}^{-3}$ during the port-anchoring period. The 25th percentile value of DMAH⁺ during Campaign A was $0.021 \mu\text{g m}^{-3}$, suggesting a low background concentration in the marine area. The DMAH⁺ concentrations were significantly correlated with those of NH₄⁺ ($R^2=0.71$, $P<0.01$; data not shown). When the data obtained at 03:00–05:59 and 14:00–16:59 on December 18 (strong peaks of TMAH⁺ with a simultaneous increase in DMAH⁺) were removed for correlation, the R^2 value improved to 0.78. Unlike the TMAH⁺, the observed DMAH⁺ may have been partially derived from acid-basic neutralization reactions in the ambient air, in addition to the primary sea-spray organic aerosols. For example, a large increase in DMAH⁺ concentrations occurred concurrently with strong peaks in the TMAH⁺ concentrations (gray shadowed peak 4 in Figs. 3a & b).

The NH₄⁺ concentrations of PM_{2.5} varied greatly at approximately $4.7 \pm 7.2 \mu\text{g m}^{-3}$ during Campaign A (Fig. 3c). However, the 25th percentile values were as low as $0.21 \mu\text{g m}^{-3}$, suggesting low marine background values. The 50th percentile value was also only $1.2 \mu\text{g m}^{-3}$, which was considerably smaller than the average owing to the presence of strong peaks in the NH₄⁺ concentrations. The increased NH₄⁺ concentrations associated with NO₃⁻ and nss-SO₄²⁻ during Campaign A were likely due to the long-range transport from the upwind continents.

4. Discussion

4.1 Effects of temperature on the observed basic gases in the marine atmosphere

As mentioned above, the observed TMA_{gas} likely originated from marine sources. We plotted the concentrations of TMA_{gas} against the ambient air temperature (T) in Fig. 4a, which generally increased with increasing T. We further separated the average hourly wind speeds (WS) into three categories, i.e.: $WS \leq 5.0$, $5.0 < WS \leq 9.0$, and $WS > 9.0 \text{ m s}^{-1}$. At $WS > 9.0 \text{ m s}^{-1}$, the data obtained from 15:00 on December 16 to 01:00 on December 19, including peaks 3 and 4, were separately considered as half-full symbols in Fig. 4a. The concentrations of TMA_{gas} (half-full symbols) generally exceeded those of the other gases at the same T, with which they exhibited a moderately good exponent correlation, $[TMA_{\text{gas}}] = 0.03 \times e^{0.04T}$ with $R^2=0.72$). From 15:00 on December 16 to 01:00 on December 19, stronger emission potentials of TMA_{gas} to the marine

atmosphere were expected in the corresponding marine zone. However, the measured concentrations of TMAH⁺ and seawater pH in the surface seawater are required to confirm this.

245 Following the same approach, the DMA_{gas} and NH_{3gas} concentrations were plotted against T, as shown in Figs. 4b & c, respectively. These values generally increased with increasing T. The NH_{3gas} concentrations (half-full symbols) were strongly correlated with T ($[\text{NH}_{3\text{gas}}] = 0.05 \times e^{0.3T}$ with $R^2=0.96$). As lower concentrations of nss-SO₄²⁻, NH₄⁺, and SO₂ were generally observed simultaneously, the continental transport of NH_{3gas} was greatly reduced; therefore, the observed NH_{3gas} was likely mainly derived from the seas. Therefore, the seas were the net source of NH_{3gas} at the time of measurement. However, at the same T, the NH_{3gas} concentrations (half-full symbols) were generally lower than those during the other periods in this study. The concentrations of NH₄⁺ in the surface seawater may have been lower at the time of measurement. 250 However, this may not be the case, as higher concentrations of TMAH⁺ were expected. Alternatively, the continental transport of NH_{3gas} may have made an important contribution to the observed NH_{3gas} during most of the other periods when the seas were the net NH_{3gas} sink.

DMA_{gas} exhibited an extremely good exponent correlation with T (half-full symbols) at the measurement time ($[\text{DMA}_{\text{gas}}] = 0.001 \times e^{0.3T}$ with $R^2=0.91$). At the same T, the DMA_{gas} concentrations (half-full symbols) were not always higher or lower than the others. We considered these two hypotheses: In hypothesis 1, the observed DMA_{gas} concentrations exceeded those predicted by the regression equation using the ambient T as the input; the seas were the likely net sinks of the DMA_{gas}. In hypothesis 2, including all others, measurements of the DMAH⁺ in the surface seawater were required to confirm whether the seas were the net sources or sinks of DMA_{gas}. 255

260 4.2 Estimating the sea-derived DMA_{gas} and NH_{3gas} in the marine atmosphere

To estimate the sea-derived DMA_{gas} and NH_{3gas} concentrations in the marine atmosphere, we plotted the DMA_{gas} and NH_{3gas} concentrations against TMA_{gas}, as shown in Figs. 5a and b. The purple-red and dark-green markers represent the data obtained, with increasing concentrations of the three species from 10:00 on December 14 to 23:00 on December 16 (increasing period), and with decreasing concentrations from 23:00 on December 16 to 19:59 on December 17 (decreasing period) during peak 3, respectively; these were analyzed separately. A good correlation was obtained between DMA_{gas} and 265

TMA_{gas} during the increasing period ($[DMA_{gas}] = 0.64 \times [TMA_{gas}] - 0.01$, $R^2=0.86$, and $P<0.01$). The good correlation suggested that DMA_{gas} was likely released with TMA_{gas} from the seawater, and facilitated the estimation of non-sea-derived DMA_{gas} (DMA_{gas}[#]) concentrations using the regression equation. We assumed that any data beyond the purple-red dashed line reflected the contribution of non-sea-derived DMA_{gas}, which can be attributed to continental transport. Therefore, we assumed that the DMA_{gas}[#] concentrations were equal to the observed values of DMA_{gas} minus the predicted values obtained using $[DMA_{gas}] = 0.64 \times [TMA_{gas}] - 0.01$; and the calculated DMA_{gas}[#] values are shown in Fig. 5c. During peak 1, the calculated DMA_{gas}[#] contributed to over 40% of the observed DMA_{gas} for 12 h. Similar calculated results for DMA_{gas}[#] were obtained during peak 2.

However, the equation for the decreasing period was as follows: $[DMA_{gas}] = 1.4 \times [TMA_{gas}] - 0.05$, $R^2=0.84$, and $P<0.01$. The decreasing R^2 value and the increasing slope suggest that the TMAH⁺ in the surface seawater may decompose into DMAH⁺ to different extents (Lidbury et al., 2015a; Lidbury et al., 2015b; Xie et al., 2018). The two regression curves (purple-red and dark-green dashed lines in Figs. 5a and b) created a large triangular zone that likely reflected the different ratios of DMA_{gas}/TMA_{gas} in primary marine emissions on the cruise route. Based on the triangular zone in Fig. 5a, the aforementioned calculations should be considered as the lower limit of DMA_{gas}[#].

The same approach was employed to analyze the NH_{3gas} results, as shown in Figs. 5b and d. During peak 1, the calculated non-sea-derived NH_{3gas} (NH_{3gas}[#]) contributed to over 40% of the observed NH_{3gas} for 17 h. During peak 2, the calculated NH_{3gas}[#] contributed to over 40% of the observed NH_{3gas} for 24 h.

Overall, the DMA_{gas}[#] and NH_{3gas}[#] concentrations varied at approximately 0.001 ± 0.002 and $0.18 \pm 0.39 \mu\text{g m}^{-3}$, respectively. The calculated average DMA_{gas}[#] and NH_{3gas}[#] values accounted for 16% and 34% of the observed averages of each species, respectively. The estimations suggested an appreciable continental contribution to the observed DMA_{gas} and NH_{3gas} during the Camping A.

4.3 Estimation of non-sea-spray particulate DMAH⁺ in the marine atmosphere

We plotted the concentrations of DMAH⁺ against those of TMAH⁺ in PM_{2.5} (Fig. 6a) using the data obtained from 15:00 on

290 December 16 to 01:00 on December 19 ($[\text{DMAH}^+]_{\text{PM}_{2.5}} = 0.13 \times [\text{TMAH}^+]_{\text{PM}_{2.5}}$, $R^2=0.91$, $P<0.01$). During this period, largely increased concentrations of DMAH^+ and TMAH^+ were observed under high wind speeds of 9-13 m s^{-1} . The good correlation suggested that the observed DMAH^+ was likely released with TMAH^+ as amines-contained sea spray aerosols in the atmosphere, and facilitated the calculation of sea-derived DMAH^+ using TMAH^+ as a tracer of sea-spray aerosols. Thus, the non-sea-derived DMAH^+ concentrations in $\text{PM}_{2.5}$, marked as $\text{DMAH}^{+\#}$, were assumed to be equal to the observed DMAH^+ values minus the predicted values (sea-derived DMAH^+) using the regression equation. The calculated $\text{DMAH}^{+\#}$ values are shown in Fig. 6b. The $\text{DMAH}^{+\#}$ concentrations varied at approximately $0.042 \pm 0.070 \mu\text{g m}^{-3}$ throughout Campaign A, during which the calculated average $\text{DMAH}^{+\#}$ accounted for 65% of the observed average. Additionally, the calculated $\text{DMAH}^{+\#}$ values accounted for over 80% of the observed values in 26% of the Campaign A period. The estimations suggested that the observed DMAH^+ originated predominantly came from the long-range continental transport and/or secondary formation in the marine atmosphere. The analysis was supported by the good correlation between the concentrations of $\text{DMAH}^{+\#}$ and those of NH_4^+ ; namely, $[\text{DMAH}^{+\#}]_{\text{PM}_{2.5}} = 0.0089 \times [\text{NH}_4^+]_{\text{PM}_{2.5}}$, ($R^2=0.82$, $P<0.01$; Fig. 6c). The slope of 0.0089 was approximately 50% larger than that obtained in the coastal atmosphere (0.0059), suggesting more DMA_{gas} partitioning in $\text{PM}_{2.5}$ in the marine atmosphere than in the coastal atmosphere (Pankow, 2015; Xie et al., 2018). Moreover, the decomposition of TMAH^+ to DMAH^+ may have occurred in surface seawater and/or the marine atmosphere, to an extent, and the estimated $\text{DMAH}^{+\#}$ should be considered as the upper limit. Notably, the NH_4^+ and TMAH^+ concentrations were negatively correlated during Campaign A, and no primary particulate NH_4^+ from sea-spray aerosols were identified.

4.4 Formation and chemical conversion of aminium ions in the transported and self-vessel SO_2 plumes

When the sea-spray particulate DMAH^+ was deducted, the increased concentrations of $\text{DMAH}^{+\#}$ were generally associated with increased nss-SO_4^{2-} and SO_2 concentrations. Combining this with the moderate correlation between $\text{DMAH}^{+\#}$ and NH_4^+ , we inferred that the $\text{DMAH}^{+\#}$ likely originated from concurrent secondary formation with NH_4^+ . However, we separated the air pollutant plumes into two groups. Group 1 represented an increase in nss-SO_4^{2-} and NH_4^+ together with SO_2 , while group 2 represented an increase in SO_2 without increases in nss-SO_4^{2-} and NH_4^+ . Group 1 likely reflected the transport of aged air

pollutant plumes from the continents, while group 2 may reflect self-vessel SO₂ plumes. As shown in Figs. 6b and 3b-c, the concentrations of DMAH^{+#} and NH₄⁺ in the self-vessel SO₂ plumes did not increase in the intervals between peaks 1 and 2, and between peaks 2 and 3. Therefore, no fresh formation of DMAH^{+#} and NH₄⁺ in the self-vessel emissions was detected. However, the concentrations of TMAH⁺ decreased in some self-vessel SO₂ plumes. The TMAH⁺ concentrations were approximately one order of magnitude higher than those of TMA_{gas} in the marine atmosphere. Assuming that the decreased TMAH⁺ was released from PM_{2.5} to the gas phase, a simultaneous large spike in TMA_{gas} should be observed. However, this was not the case, as shown in Fig. 1c. The decreased TMAH⁺ may persist in the PM_{2.5}, but could not be detected by AIM-IC.

5. Conclusion and Implication

In continental China upwind of the Yellow Sea, the TMA_{gas} and TMAH⁺ concentrations in PM_{2.5} were extremely low (0.001±0.001 μg m⁻³), mostly below the detection limit of the AIM-IC. Considering the observations as a reference, the largely increased TMA_{gas} (0.031±0.009 μg m⁻³) and particulate TMAH⁺ (0.28±0.18 μg m⁻³) concentrations in the marine atmosphere were attributed to marine emissions. Therefore, TMA_{gas} and particulate TMAH⁺ can be used as unique tracers to quantify the marine emissions of DMA_{gas}, NH_{3gas}, and particulate DMAH⁺, as well as the long-range transport from upwind continental China.

Through comprehensive comparison and correlation analyses, the high concentrations of TMAH⁺ in PM_{2.5} observed over the Yellow and Bohai seas, with episodic hourly averages exceeding over 1 μg m⁻³, were inferred to originate from strong primary sea-spray aerosol emissions. Moreover, the TMA_{gas} concentrations generally increased with increasing ambient temperature and sea surface wind speeds, suggesting that the observed TMA_{gas} was likely released from the surface seawater. However, the TMA_{gas} concentrations were substantially lower than those of particulate TMAH⁺, and were not significantly correlated. Although different mechanisms have been reported in the literature for the release of TMA_{gas} and particulate TMAH⁺ from the seas have been reported in the literature, the lack of a significant correlation between them was surprising and was explored in the companion study.

The DMA_{gas} and NH_{3gas} concentrations varied at approximately 0.006±0.006 and 0.53±0.53 μg m⁻³ during Campaign A, wherein at least 16% and 34% of the observational values were derived from continental transport, respectively. The sea-

derived DMA_{gas} and NH_{3gas} were likely released with TMA_{gas} as they peaked simultaneously. The DMAH⁺ concentrations in PM_{2.5} varied at approximately 0.065±0.068 µg m⁻³ during Campaign A, 65% of which was derived from continental transport.

Our analysis results did not support the occurrence of the photolysis of marine organic nitrogen to generate NH_{3gas} in the marine atmosphere during winter, as there was no correlation between the sea-derived NH_{3gas} and particulate TMAH⁺ concentrations. Additionally, peaks 2 and 3 of NH_{3gas} persisted for dozens of hours under strong winds and were therefore unlikely to be derived from seabird emissions. A good exponent correlation was observed between the observed NH_{3gas} concentrations and T during the period without continental air pollutant transport, suggesting that the observed NH_{3gas} was released from seawater. NH₃ emissions from seabirds were unlikely contributors to the observed NH_{3gas} in the marine atmosphere during winter; however, this may not have been the case during other seasons.

Additionally, no formation of particulate NH₄⁺ and DMAH⁺ in the self-vessel SO₂ plume was observed in the marine atmosphere. However, the particulate TMAH⁺ concentration clearly decreased in the self-vessel SO₂ plume without a simultaneous increase in the TMA_{gas} concentration. Chemical conversion of particulate TMAH⁺ likely occurred in the plume, while the AIM-IC could not detect the products. This requires further investigation.

Data availability. The data of this paper are available upon request (contact: Xiaohong Yao, xhyao@ouc.edu.cn).

Acknowledgment

This research is supported by the Natural Science Foundation of China (grant no. 41776086), the National Key Research and Development Program in China (grant no. 2016YFC0200504), the Fundamental Research Funds for the Central Universities (202072002).

References

Almeida, J., Schobesberger, S., Kürten, A., Ortega, I. K., Kupiainen-Määttä, O., Praplan, A. P., Adamov, A., Amorim, A., Bianchi, F., Breitenlechner, M., David, A., Dommen, J., Donahue, N. M., Downard, A., Dunne, E., Duplissy, J., Ehrhart, S., Flagan, R. C., Franchin, A., Guida, R., Hakala, J., Hansel, A., Heinritzi, M., Henschel, H., Jokinen, T., Junninen, H.,

Kajos, M., Kangasluoma, J., Keskinen, H., Kupc, A., Kurtén, T., Kvashin, A. N., Laaksonen, A., Lehtipalo, K.,
Leiminger, M., Leppä, J., Loukonen, V., Makhmutov, V., Mathot, S., McGrath, M. J., Nieminen, T., Olenius, T., Onnela,
A., Petäjä, T., Riccobono, F., Riipinen, I., Rissanen, M., Rondo, L., Ruuskanen, T., Santos, F. D., Sarnela, N., Schallhart,
S., Schnitzhofer, R., Seinfeld, J. H., Simon, M., Sipilä, M., Stozhkov, Y., Stratmann, F., Tomé, A., Tröstl, J.,
365 Tsagkogeorgas, G., Vaattovaara, P., Viisanen, Y., Virtanen, A., Vrtala, A., Wagner, P. E., Weingartner, E., Wex, H.,
Williamson, C., Wimmer, D., Ye, P., Yli-Juuti, T., Carslaw, K. S., Kulmala, M., Curtius, J., Baltensperger, U., Worsnop,
D. R., Vehkamäki, H., and Kirkby, J.: Molecular understanding of sulphuric acid–amine particle nucleation in the
atmosphere, *Nature*, 502, 359–363, <https://doi.org/10.1038/nature12663>, 2013.

Ault, A. P., Moffet, R. C., Baltrusaitis, J., Collins, D. B., Ruppel, M. J., Cuadra-Rodriguez, L. A., Zhao, D., Guasco, T. L.,
370 Ebben, C. J., Geiger, F. M., Bertram, T. H., Prather, K. A., and Grassian, V. H.: Size-dependent changes in sea spray
aerosol composition and properties with different seawater conditions, *Environmental Science & Technology*, 47, 5603–
5612, <https://doi.org/10.1021/es400416g>, 2013.

Burg, M. B. and Ferraris, J. D.: Intracellular organic osmolytes: Function and regulation, *Journal of Biological Chemistry*,
283, 7309–7313, <https://doi.org/10.1074/jbc.R700042200>, 2008.

375 Carpenter, L. J., Archer, S. D., and Beale, R.: Ocean-atmosphere trace gas exchange, *Chem. Soc. Rev.*, 41, 6473–6506,
<https://doi.org/10.1039/C2CS35121H>, 2012.

Chen, H., Varner, M. E., Gerber, R. B., and Finlayson-Pitts, B. J.: Reactions of methanesulfonic acid with amines and
ammonia as a source of new particles in air, *The Journal of Physical Chemistry B*, 120, 1526–1536,
<https://doi.org/10.1021/acs.jpcc.5b07433>, 2016.

380 Clarke, A. D. and Porter, J. N.: Pacific marine aerosol: 2. Equatorial gradients in chlorophyll, ammonium, and excess sulfate
during SAGA 3, *J. Geophys. Res.*, 98, 16997–17010, <https://doi.org/10.1029/92JD02481>, 1993.

Dall’Osto, M., Airs, R. L., Beale, R., Cree, C., Fitzsimons, M. F., Beddows, D., Harrison, R. M., Ceburnis, D., O’Dowd, C.,
Rinaldi, M., Paglione, M., Nenes, A., Decesari, S., and Simó, R.: Simultaneous detection of alkylamines in the surface
ocean and atmosphere of the Antarctic sympagic environment, *ACS Earth and Space Chemistry*, 3, 854–862,

385 <https://doi.org/10.1021/acsearthspacechem.9b00028>, 2019.

- Deng, Y., Gao, T., Gao, H., Yao, X., and Xie, L.: Regional precipitation variability in East Asia related to climate and environmental factors during 1979-2012, *Sci Rep*, 4, 5693, <https://doi.org/10.1038/srep05693>, 2014.
- Dentener, F. J. and Crutzen, P. J.: A three-dimensional model of the global ammonia cycle, *Journal of Atmospheric Chemistry*, 19, 331–369, <https://doi.org/10.1007/BF00694492>, 1994.
- 390 Facchini, M. C., Decesari, S., Rinaldi, M., Carbone, C., Finessi, E., Mircea, M., Fuzzi, S., Moretti, F., Tagliavini, E., Ceburnis, D., and O’Dowd, C. D.: Important source of marine secondary organic aerosol from biogenic amines, *Environmental Science & Technology*, 42, 9116–9121, <https://doi.org/10.1021/es8018385>, 2008.
- Feng, L., Shen, H., Zhu, Y., Gao, H., and Yao, X.: Insight into generation and evolution of sea-salt aerosols from field measurements in diversified marine and coastal atmospheres, *Scientific Reports*, 7, 41260, <https://doi.org/10.1038/srep41260>, 2017.
- 395 Gao, Y., Chen, D., Shen, Y., Gao, Y., Gao, H., and Yao, X.: Mapping gaseous amines, ammonia and their particulate counterparts in marine atmospheres of China's marginal seas: Part 2 - spatiotemporal heterogeneity, causes and hypothesis, *Atmos. Chem. Phys. Discuss.* [preprint], <https://doi.org/10.5194/acp-2021-301>, in review, 2021.
- Gibb, S. W., Mantoura, R. F. C., and Liss, P. S.: Ocean-atmosphere exchange and atmospheric speciation of ammonia and methylamines in the region of the NW Arabian Sea, *Global Biogeochemical Cycle*, 13, 161–178, <https://doi.org/10.1029/98GB00743>, 1999.
- 400
- Guo, C., Zhang, G., Sun, J., Leng, X., Xu, W., Wu, C., Li, X., and Pujari, L.: Seasonal responses of nutrient to hydrology and biology in the southern Yellow Sea, *Continental Shelf Research*, 206, 104207, <https://doi.org/10.1016/j.csr.2020.104207>, 2020.
- 405 Guo, T., Li, K., Zhu, Y., Gao, H., and Yao, X.: Concentration and size distribution of particulate oxalate in marine and coastal atmospheres – Implication for the increased importance of oxalate in nanometer atmospheric particles, *Atmospheric Environment*, 142, 19–31, <https://doi.org/10.1016/j.atmosenv.2016.07.026>, 2016.
- Hu, Q., Qu, K., Gao, H., Cui, Z., Gao, Y., and Yao, X.: Large increases in primary trimethylaminium and secondary dimethylaminium in atmospheric particles associated with cyclonic eddies in the northwest Pacific Ocean, *Journal of Geophysical Research: Atmospheres*, 123, 12,133-12,146, <https://doi.org/10.1029/2018JD028836>, 2018.
- 410

- Hu, Q., Yu, P., Zhu, Y., Li, K., Gao, H., and Yao, X.: Concentration, size distribution, and formation of trimethylammonium and dimethylammonium ions in atmospheric particles over marginal seas of China, *Journal of the Atmospheric Sciences*, 72, 3487–3498, <https://doi.org/10.1175/JAS-D-14-0393.1>, 2015.
- Jameson, E., Doxey, A. C., Airs, R., Purdy, K. J., Murrell, J. C., and Chen, Y.: Metagenomic data-mining reveals contrasting microbial populations responsible for trimethylamine formation in human gut and marine ecosystems, *Microbial Genomics*, 2, <https://doi.org/10.1099/mgen.0.000080>, 2016.
- Johnson, M. T., Liss, P. S., Bell, T. G., Lesworth, T. J., Baker, A. R., Hind, A. J., Jickells, T. D., Biswas, K. F., Woodward, E. M. S., and Gibb, S. W.: Field observations of the ocean-atmosphere exchange of ammonia: Fundamental importance of temperature as revealed by a comparison of high and low latitudes, *Global Biogeochem. Cycles*, 22, <https://doi.org/10.1029/2007GB003039>, 2008.
- Keene, W. C., Long, M. S., Pszenny, A. A. P., Sander, R., Maben, J. R., Wall, A. J., O’Halloran, T. L., Kerkweg, A., Fischer, E. V., and Schrems, O.: Latitudinal variation in the multiphase chemical processing of inorganic halogens and related species over the eastern North and South Atlantic Oceans, *Atmospheric Chemistry and Physics*, 9, 7361–7385, <https://doi.org/10.5194/acp-9-7361-2009>, 2009.
- Lidbury, I., Kimberley, G., Scanlan, D. J., Murrell, J. C., and Chen, Y.: Comparative genomics and mutagenesis analyses of choline metabolism in the marine *Roseobacter* clade, *Environ Microbiol*, 17, 5048–5062, <https://doi.org/10.1111/1462-2920.12943>, 2015a.
- Lidbury, I. D., Murrell, J. C., and Chen, Y.: Trimethylamine and trimethylamine N-oxide are supplementary energy sources for a marine heterotrophic bacterium: Implications for marine carbon and nitrogen cycling, *The ISME Journal*, 9, 760–769, <https://doi.org/10.1038/ismej.2014.149>, 2015b.
- Lutsch, E., Dammers, E., Conway, S., and Strong, K.: Long-range transport of NH₃, CO, HCN, and C₂H₆ from the 2014 Canadian wildfires, *Geophysical Research Letters*, 43, 8286–8297, <https://doi.org/10.1002/2016GL070114>, 2016.
- Mao, J., Yu, F., Zhang, Y., An, J., Wang, L., Zheng, J., Yao, L., Luo, G., Ma, W., Yu, Q., Huang, C., Li, L., and Chen, L.: High-resolution modeling of gaseous methylamines over a polluted region in China: source-dependent emissions and implications of spatial variations, *Atmospheric Chemistry and Physics*, 18, 7933–7950, <https://doi.org/10.5194/acp-18->

- McNaughton, C. S., Clarke, A. D., Howell, S. G., Moore II, K. G., Brekhovskikh, V., Weber, R. J., Orsini, D. A., Covert, D. S., Buzorius, G., Brechtel, F. J., Carmichael, G. R., Tang, Y., Eisele, F. L., Mauldin, R. L., Bandy, A. R., Thornton, D. C., and Blomquist, B.: Spatial distribution and size evolution of particles in Asian outflow: Significance of primary and secondary aerosols during ACE-Asia and TRACE-P, *Journal of Geophysical Research: Atmospheres*, 109, 440 <https://doi.org/10.1029/2003JD003528>, 2004.
- Müller, C., Iinuma, Y., Karstensen, J., van Pinxteren, D., Lehmann, S., Gnauk, T., and Herrmann, H.: Seasonal variation of aliphatic amines in marine sub-micrometer particles at the Cape Verde islands, *Atmospheric Chemistry and Physics*, 9, 9587–9597, <https://doi.org/10.5194/acp-9-9587-2009>, available at: <https://acp.copernicus.org/articles/9/9587/2009/>, 445 2009.
- Pankow, J. F.: Phase considerations in the gas/particle partitioning of organic amines in the atmosphere, *Atmospheric Environment*, 122, 448–453, <https://doi.org/10.1016/j.atmosenv.2015.09.056>, 2015.
- Paulot, F., Jacob, D. J., Johnson, M. T., Bell, T. G., Baker, A. R., Keene, W. C., Lima, I. D., Doney, S. C., and Stock, C. A.: Global oceanic emission of ammonia: Constraints from seawater and atmospheric observations, *Global Biogeochem. Cycles*, 29, 1165–1178, <https://doi.org/10.1002/2015GB005106>, 2015. 450
- Prather, K. A., Bertram, T. H., Grassian, V. H., Deane, G. B., Stokes, M. D., Demott, P. J., Aluwihare, L. I., Palenik, B. P., Azam, F., Seinfeld, J. H., Moffet, R. C., Molina, M. J., Cappa, C. D., Geiger, F. M., Roberts, G. C., Russell, L. M., Ault, A. P., Baltrusaitis, J., Collins, D. B., Corrigan, C. E., Cuadra-Rodriguez, L. A., Ebben, C. J., Forestieri, S. D., Guasco, T. L., Hersey, S. P., Kim, M. J., Lambert, W. F., Modini, R. L., Mui, W., Pedler, B. E., Ruppel, M. J., Ryder, O. S., 455 Schoepp, N. G., Sullivan, R. C., and Zhao, D.: Bringing the ocean into the laboratory to probe the chemical complexity of sea spray aerosol, *Proc Natl Acad Sci U S A*, 110, 7550–7555, <https://doi.org/10.1073/pnas.1300262110>, 2013.
- Quinn, P. K., Collins, D. B., Grassian, V. H., Prather, K. A., and Bates, T. S.: Chemistry and related properties of freshly emitted sea spray aerosol, *Chemical Reviews*, 115, 4383–4399, <https://doi.org/10.1021/cr500713g>, 2015.
- Quinn, P. K., Bates, T. S., Johnson, J. E., Covert, D. S., and Charlson, R. J.: Interactions between the sulfur and reduced 460 nitrogen cycles over the central Pacific Ocean, *J. Geophys. Res.*, 95, 16405–16416,

<https://doi.org/10.1029/JD095iD10p16405>, 1990.

Sutton, M. A., Reis, S., Riddick, S. N., Dragosits, U., Nemitz, E., Theobald, M. R., Tang, Y. S., Braban, C. F., Vieno, M., Dore, A. J., Mitchell, R. F., Wanless, S., Daunt, F., Fowler, D., Blackall, T. D., Milford, C., Flechard, C. R., Loubet, B., Massad, R., Cellier, P., Personne, E., Coheur, P. F., Clarisse, L., van Damme, M., Ngadi, Y., Clerbaux, C., Skj  th, C. A., Geels, C., Hertel, O., Wichink Kruit, R. J., Pinder, R. W., Bash, J. O., Walker, J. T., Simpson, D., Horv  th, L., Misselbrook, T. H., Bleeker, A., Dentener, F., and Vries, W. de: Towards a climate-dependent paradigm of ammonia emission and deposition, *Philosophical Transactions of the Royal Society B: Biological Sciences*, 368, 20130166, <https://doi.org/10.1098/rstb.2013.0166>, 2013.

Taubert, M., Grob, C., Howat, A. M., Burns, O. J., Pratscher, J., Jehmlich, N., Bergen, M. von, Richnow, H. H., Chen, Y., and Murrell, J. C.: Methylamine as a nitrogen source for microorganisms from a coastal marine environment, *Environmental Microbiol*, 19, 2246–2257, <https://doi.org/10.1111/1462-2920.13709>, 2017.

Teng, X., Hu, Q., Zhang, L., Qi, J., Shi, J., Xie, H., Gao, H., and Yao, X.: Identification of major sources of atmospheric NH₃ in an urban environment in northern China during wintertime, *Environmental Science & Technology*, 51, 6839–6848, <https://doi.org/10.1021/acs.est.7b00328>, 2017.

Uematsu, M., Toratani, M., Kajino, M., Narita, Y., Senga, Y., and Kimoto, T.: Enhancement of primary productivity in the western North Pacific caused by the eruption of the Miyake-jima Volcano, *Geophysical Research Letters*, 31, <https://doi.org/10.1029/2003GL018790>, 2004.

van Pinxteren, M., Fomba, K. W., van Pinxteren, D., Triesch, N., Hoffmann, E. H., Cree, C. H.L., Fitzsimons, M. F., T  mpling, W. von, and Herrmann, H.: Aliphatic amines at the Cape Verde Atmospheric Observatory: Abundance, origins and sea-air fluxes, *Atmospheric Environment*, 203, 183–195, <https://doi.org/10.1016/j.atmosenv.2019.02.011>, 2019.

van Pinxteren, M., Fiedler, B., van Pinxteren, D., Iinuma, Y., K  rtzinger, A., and Herrmann, H.: Chemical characterization of sub-micrometer aerosol particles in the tropical Atlantic Ocean: Marine and biomass burning influences, *Journal of Atmospheric Chemistry*, 72, 105–125, <https://doi.org/10.1007/s10874-015-9307-3>, 2015.

VandenBoer, T. C., Petroff, A., Markovic, M. Z., and Murphy, J. G.: Size distribution of alkyl amines in continental

particulate matter and their online detection in the gas and particle phase, *Atmospheric Chemistry and Physics*, 11, 4319–4332, <https://doi.org/10.5194/acp-11-4319-2011>, 2011.

Wang, B., Chen, Y., Zhou, S., Li, H., Wang, F., and Yang, T.: The influence of terrestrial transport on visibility and aerosol properties over the coastal East China Sea, *Science of The Total Environment*, 649, 652–660,

490 <https://doi.org/10.1016/j.scitotenv.2018.08.312>, 2019.

Wentworth, G. R., Murphy, J. G., Benedict, K. B., Bangs, E. J., and Collett Jr., J. L.: The role of dew as a night-time reservoir and morning source for atmospheric ammonia, *Atmospheric Chemistry and Physics*, 16, 7435–7449,

<https://doi.org/10.5194/acp-16-7435-2016>, 2016.

Xie, H., Feng, L., Hu, Q., Zhu, Y., Gao, H., Gao, Y., and Yao, X.: Concentration and size distribution of water-extracted dimethylammonium and trimethylammonium in atmospheric particles during nine campaigns - Implications for sources,

495 phase states and formation pathways, *Science of The Total Environment*, 631-632, 130–141,

<https://doi.org/10.1016/j.scitotenv.2018.02.303>, 2018.

Yao, L., Garmash, O., Bianchi, F., Zheng, J., Yan, C., Kontkanen, J., Junninen, H., Mazon, S. B., Ehn, M., Paasonen, P., Sipilä, M., Wang, M., Wang, X., Xiao, S., Chen, H., Lu, Y., Zhang, B., Wang, D., Fu, Q., Geng, F., Li, L., Wang, H.,

500 Qiao, L., Yang, X., Chen, J., Kerminen, V.-M., Petäjä, T., Worsnop, D. R., Kulmala, M., and Wang, L.: Atmospheric new particle formation from sulfuric acid and amines in a Chinese megacity, *Science*, 361, 278–281,

<https://doi.org/10.1126/science.aao4839>, 2018.

Yu, F., and Luo, G.: Modeling of gaseous methylamines in the global atmosphere: impacts of oxidation and aerosol uptake, *Atmospheric Chemistry and Physics*, 14, 12455–12464, <https://doi.org/10.5194/acp-14-12455-2014>, 2014

505 Yu, P., Hu, Q., Li, K., Zhu, Y., Liu, X., Gao, H., and Yao, X.: Characteristics of dimethylammonium and trimethylammonium in atmospheric particles ranging from supermicron to nanometer sizes over eutrophic marginal seas of China and

oligotrophic open oceans, *Science of The Total Environment*, 572, 813–824,

<https://doi.org/10.1016/j.scitotenv.2016.07.114>, 2016.

Zhao, Y., Zhang, L., Pan, Y., Wang, Y., Paulot, F., and Henze, D. K.: Atmospheric nitrogen deposition to the northwestern

510 Pacific: seasonal variation and source attribution, *Atmospheric Chemistry and Physics*, 15, 10905–10924,

<https://doi.org/10.5194/acp-15-10905-2015>, 2015.

Zhou, S., Li, H., Yang, T., Chen, Y., Deng, C., Gao, Y., Chen, C., and Xu, J.: Characteristics and sources of aerosol aminiums over the eastern coast of China: Insights from the integrated observations in a coastal city, adjacent island and surrounding marginal seas, *Atmospheric Chemistry and Physics*, 19, 10447–10467, <https://doi.org/10.5194/acp-19-10447-2019>, 2019.

515

Zhu, J., Shi, J., Guo, X., Gao, H., and Yao, X.: Air-sea heat flux control on the Yellow Sea Cold Water Mass intensity and implications for its prediction, *Continental Shelf Research*, 152, 14–26, <https://doi.org/10.1016/j.csr.2017.10.006>, 2018.

Zhu, Y., Li, K., Shen, Y., Gao, Y., Liu, X., Yu, Y., Gao, H., and Yao, X.: New particle formation in the marine atmosphere during seven cruise campaigns, *Atmospheric Chemistry and Physics*, 19, 89–113, <https://doi.org/10.5194/acp-19-89-2019>,

520 2019.

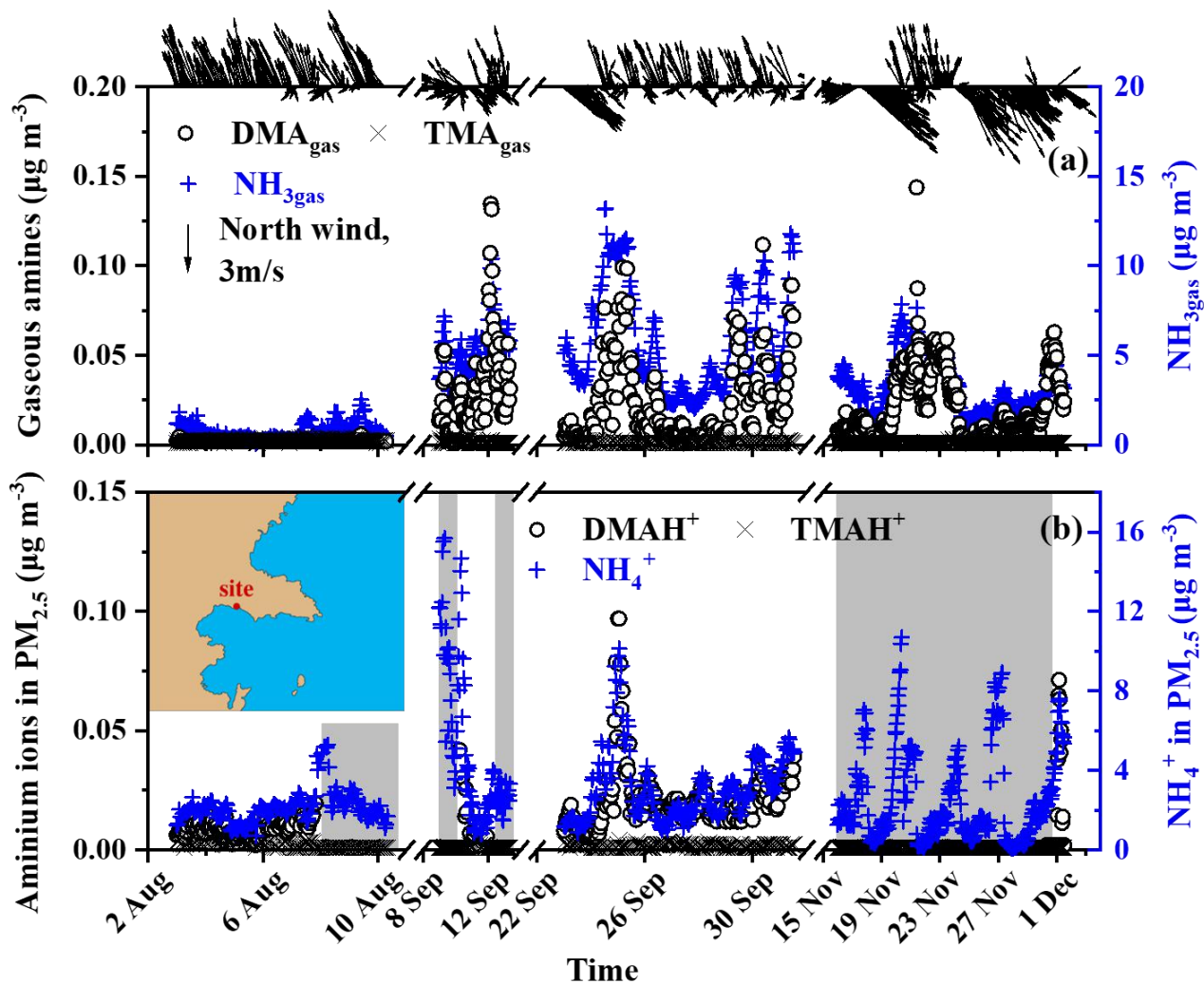


Figure 1: Temporal variations in the concentrations of NH_3gas , gaseous amines, and their counterparts in $\text{PM}_{2.5}$ at a coastal site during three seasons of 2019 ((a) NH_3gas and gaseous amines; (b) counterparts in $\text{PM}_{2.5}$; wind speed and direction superimposed on the top of (a); a map of the sampling site superimposed in (b); the missing data regarding aminium ions in the $\text{PM}_{2.5}$ shading in the gray shadow were due to occasional K^+ interference (b)).

525

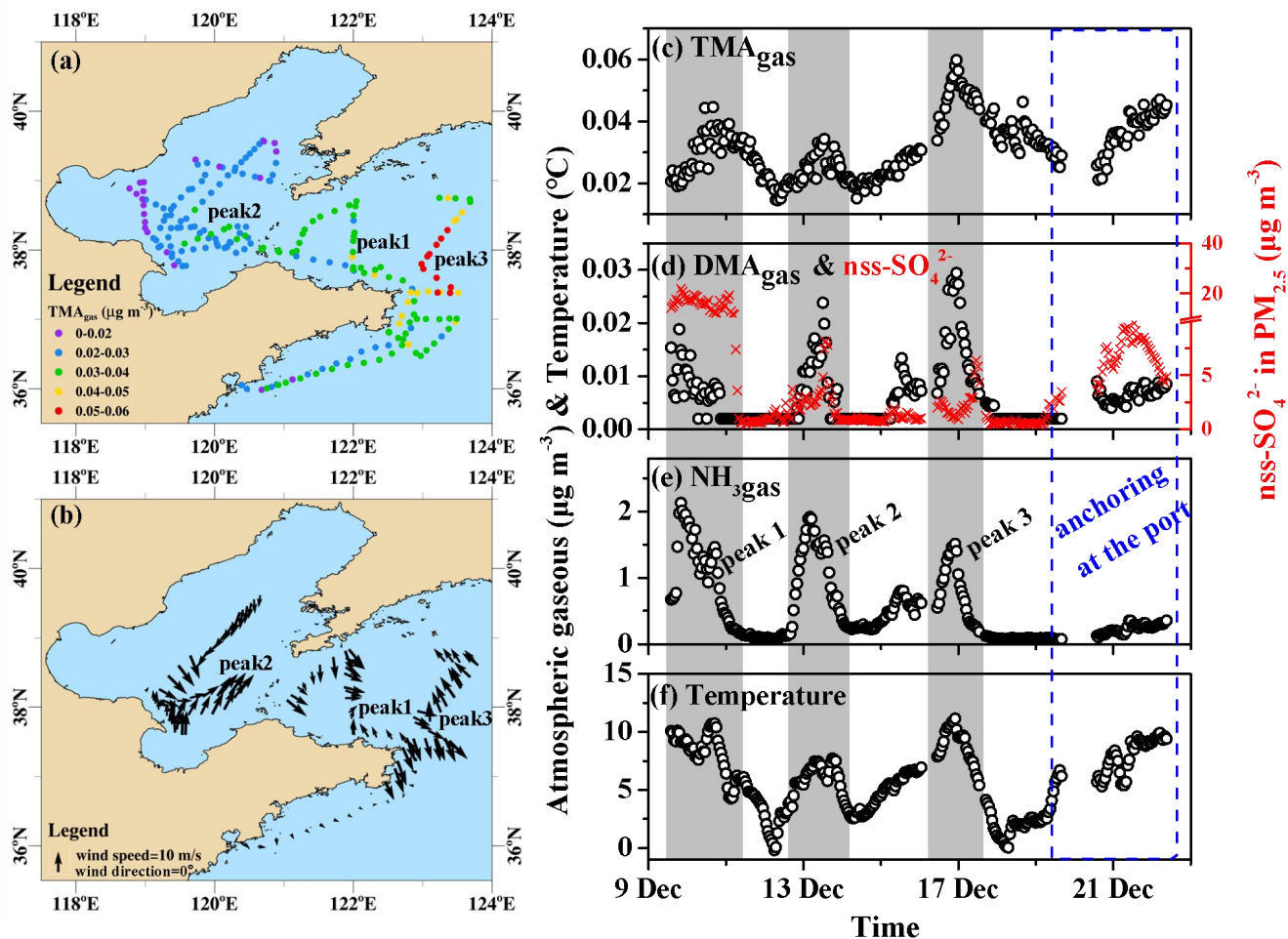


Figure 2: Spatiotemporal variations in the concentrations of basic gases and other parameters during **cruise campaigns in the Yellow and Bohai seas** on December 9-22, 2019 ((a) mapping TMA_{gas} by concentration; (b) mapping onboard recorded wind speeds and directions; time-series of (c) TMA_{gas}, (d) DMA_{gas}, (e) NH₃gas, and (f) ambient air temperature recorded onboard. The time-series of nss-SO₄²⁻ in PM_{2.5} were shown as indicators of anthropogenic air pollutants in (d); not all data were shown in (b) to avoid clustering).

530

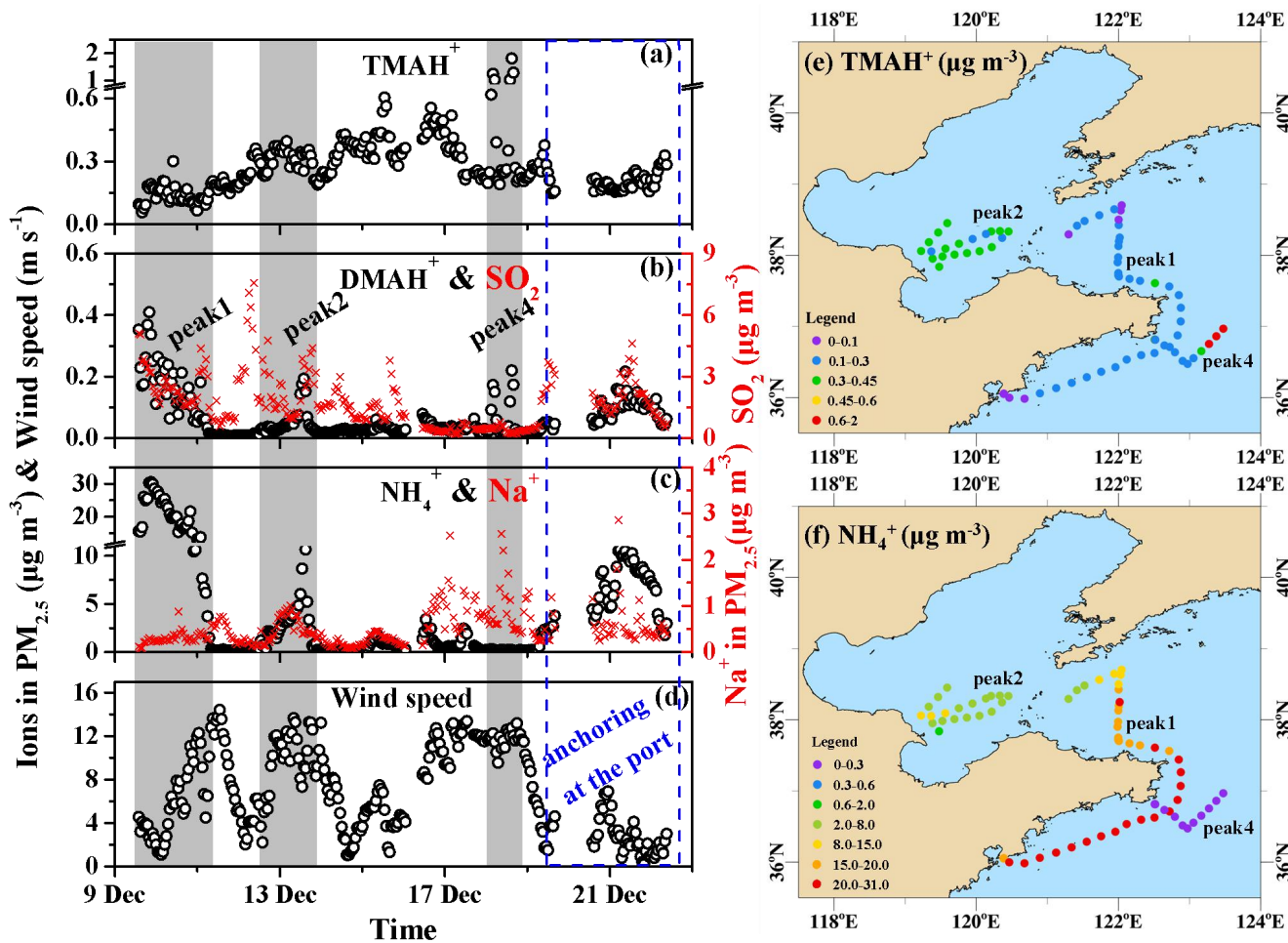
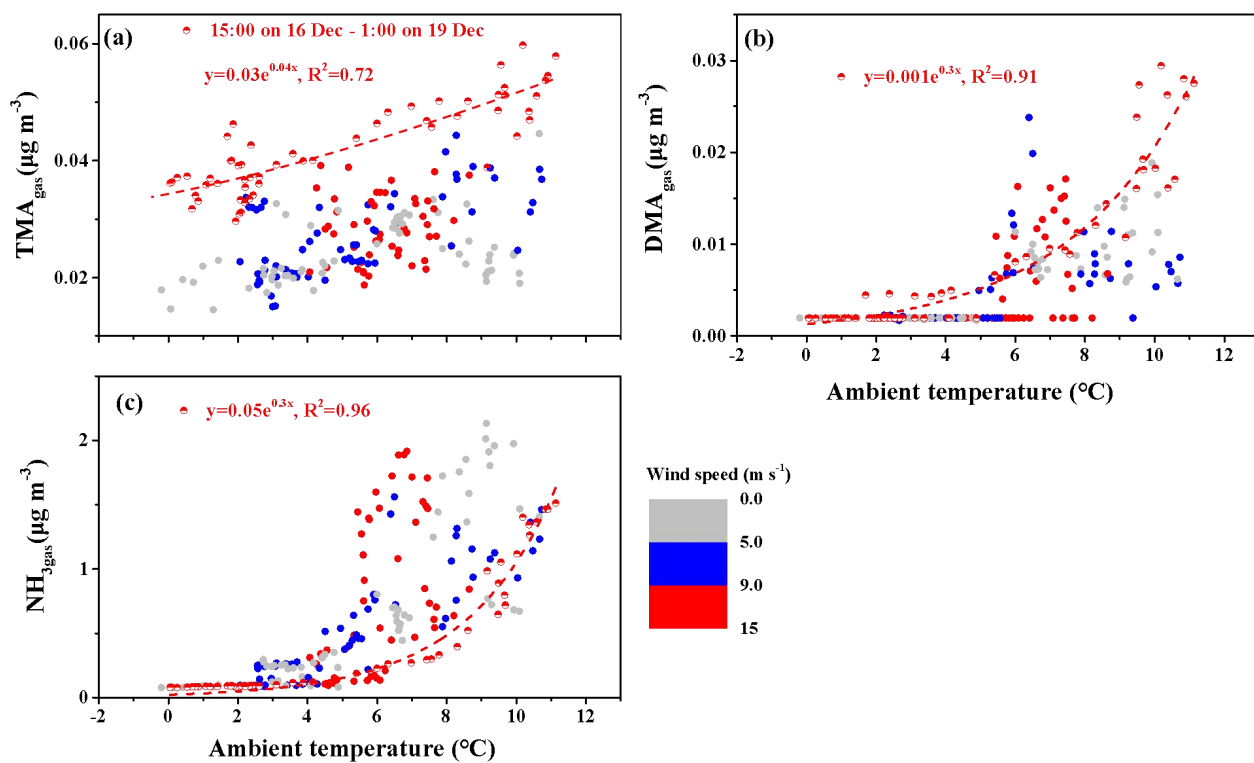


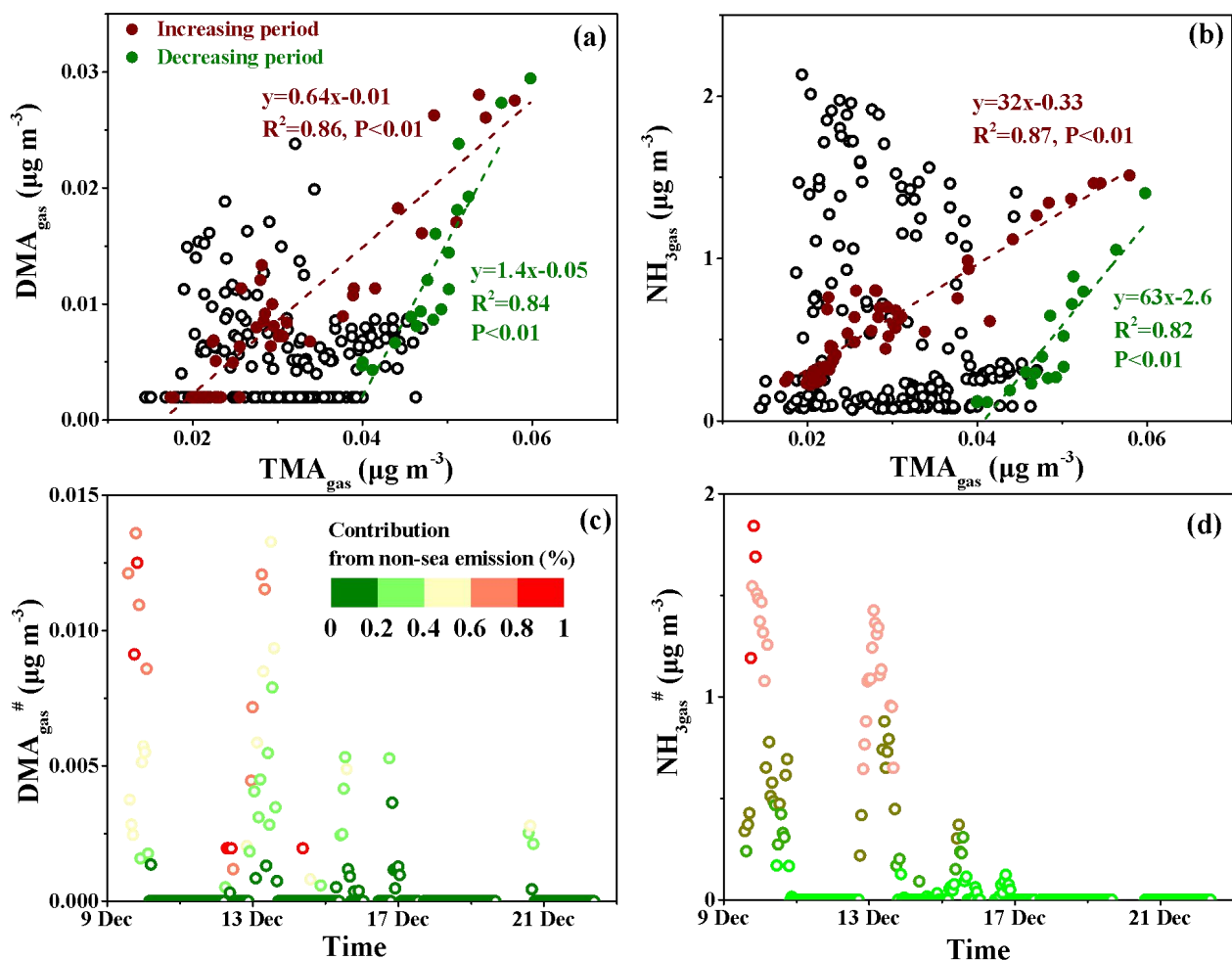
Figure 3: Spatiotemporal variations in the aminium ions and NH_4^+ concentrations of $\text{PM}_{2.5}$ and other parameters during the cruise campaigns over the Yellow and Bohai seas on December 9-22, 2019 (time-series of (a) TMAH^+ , (b) DMAH^+ , and (c) NH_4^+ in $\text{PM}_{2.5}$; (d) wind speeds (WS); (e) mapping of the TMAH^+ in concentration; (f) mapping of the NH_4^+ concentration. The time-series of SO_2 is shown as an indicator in (b); that of Na^+ in $\text{PM}_{2.5}$ is shown as an indicator of sea-spray aerosols in (c). To better show the spatiotemporal distributions of TMAH^+ and NH_4^+ during peaks 1, 2, and 4, only the data during periods shaded in (a-d) were used in (e) and (f) to avoid clustering).

535

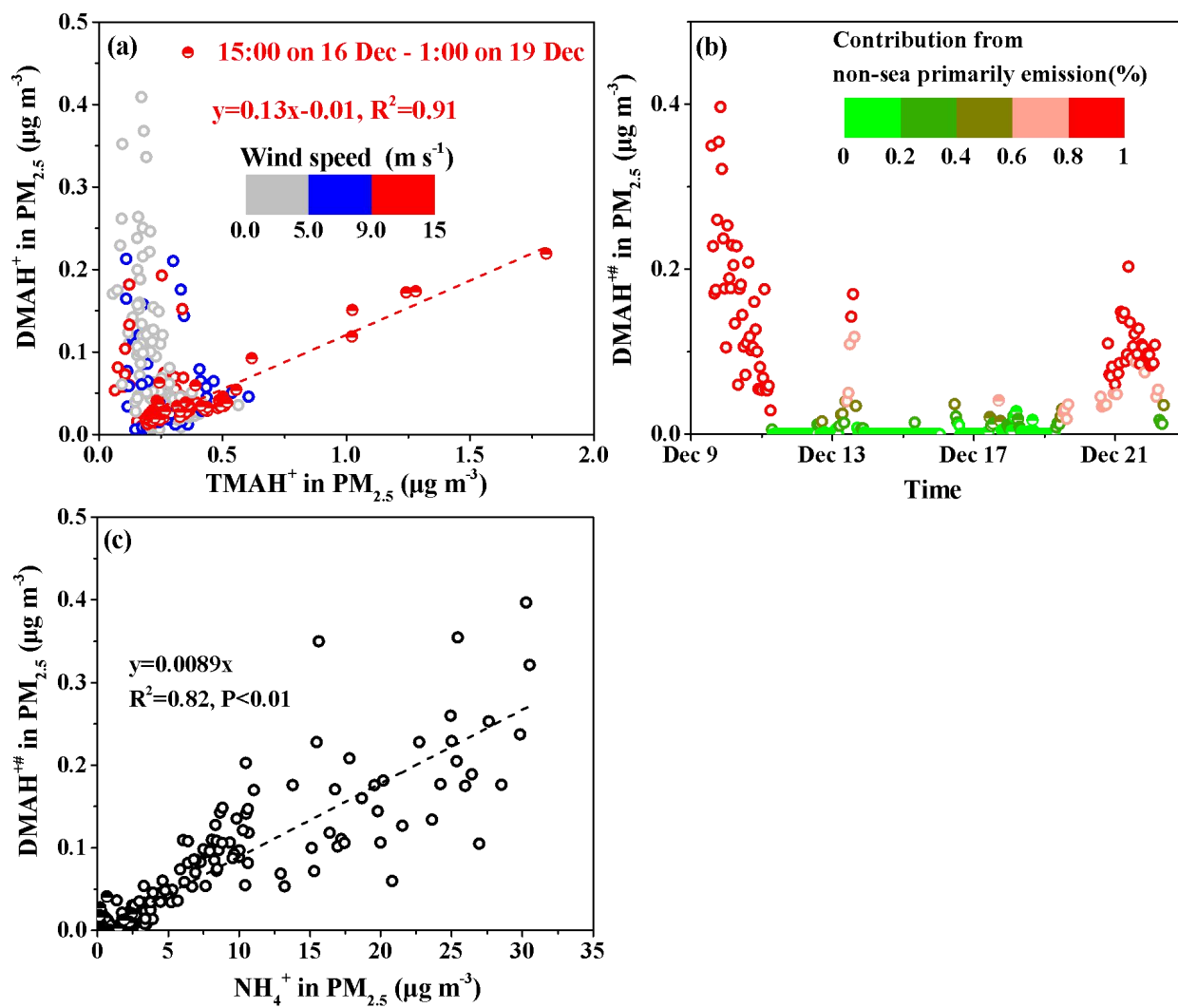


540

Figure 4: Correlations between the concentrations of basic gases and ambient temperature ((a) TMA_{gas}; (b) DMA_{gas}; (c) and NH₃). The colored bar represents different wind speeds; full symbols represent the data observed throughout the campaign excluding the period from 15:00 on December 16 to 01:00 on December 19, 2019).



545 **Figure 5: Correlations of DMA_{gas} and $\text{NH}_{3\text{gas}}$ with TMA_{gas} and time-series of the calculated $\text{DMA}_{\text{gas}}^{\#}$ and $\text{NH}_{3\text{gas}}^{\#}$ ((a) DMA_{gas} vs. TMA_{gas} ; (b) $\text{NH}_{3\text{gas}}$ vs. TMA_{gas} ; (c) $\text{DMA}_{\text{gas}}^{\#}$; and (d) $\text{NH}_{3\text{gas}}^{\#}$. The colored bars in (c) and (d) represent the percentages of transported $\text{DMA}_{\text{gas}}^{\#}$ and $\text{NH}_{3\text{gas}}^{\#}$ in each corresponding observed value).**



550 Figure 6: Correlation analyses of different variables in PM_{2.5} and the time-series of the calculated DMAH⁺ in PM_{2.5} ((a) DMAH⁺ vs. TMAH⁺; (b) time-series of DMAH⁺; (c) DMAH⁺ vs. NH₄⁺).